KKU RESEARCH JOURNAL (GRADUATE STUDY)
Vol. 17 NO. 1: January-March 2017

Condensation of H_2O_2—H_2O—Air Exhaust Gas Through Four In-Line Tube Bundles in a Heat Exchanger

การควบแน่นของก๊าซเสียที่ประกอบด้วย ไฮโดรเจนเปอร์ออกไซด์-น้ำ-อากาศ เมื่อไหลผ่านชุดแลกเปลี่ยนความร้อนที่ประกอบด้วยสี่กลุ่มท่อในแนวตรง

Sittipong Boonkaew (สิทธิพงษ์ บุญแก้ว)[1]*
Dr.Wirogana Ruengphrathuengsuka (ดร.วิโรจน์ เรืองประเทืองสุข)**
Dr.Worachest Pirompugd (ดร.วรเชษฐ์ ภิรมย์ภักดิ์)***

ABSTRACT

This study was aimed to investigate the condensation of hydrogen peroxide vapor (H_2O_2) and water vapor (H_2O) in exhaust gases, when flowing through a tube-type heat exchanger with four in-line tube bundles in a cross-flow direction. It was investigated from a test-rig and compared with the results from the computation model study in ANSYS Fluent software. The experimental results showed condensation rates inside the heat exchanger increased with the increase in the cold water flow rate, or decreased in the cooling water temperature. In addition, the maximum hydrogen peroxide concentration in the condensed liquid increased with increases in the cold water flow rate and temperature. These findings described herein, on the condensation of hydrogen peroxide resulted in decreasing concentration of hydrogen peroxide in exhaust gases. It may help to reduce the negatives impact on the environment and human health. It may also can reduce the cost in the aseptic food process.

บทคัดย่อ

การศึกษานี้มีวัตถุประสงค์เพื่อศึกษาการควบแน่นของไฮโดรเจนเปอร์ออกไซด์ (H_2O_2) และไอน้ำ (H_2O) ในก๊าซเสียที่ไหลผ่านชุดแลกเปลี่ยนความร้อนแบบท่อซึ่งมีชุดท่อสี่ชุดจัดวางอยู่ในแนวเดียวกัน โดยได้ทำการทดสอบกับชุดทดลองและทำการเปรียบเทียบผลกับผลที่ได้จากการศึกษาแบบจำลองในโปรแกรม ANSYS Fluent ผลการทดลองแสดงให้เห็นว่า อัตราการควบแน่นภายในชุดแลกเปลี่ยนความร้อนเพิ่มขึ้นเมื่ออัตราการไหลของน้ำเย็นเพิ่มขึ้น หรือเมื่อลดอุณหภูมิของน้ำเย็นต่ำลง ความเข้มข้นของไฮโดรเจนเปอร์ออกไซด์ที่ได้จากการควบแน่นจะเพิ่มขึ้นเมื่ออัตราการไหลหรืออุณหภูมิของน้ำเย็นเพิ่มขึ้น การค้นพบนี้อธิบายได้ว่า การควบแน่นของไฮโดรเจนเปอร์ออกไซด์ทำให้ก๊าซเสียมีความเข้มข้นของไฮโดรเจนเปอร์ออกไซด์ลดลง ซึ่งสามารถลดผลกระทบต่อสิ่งแวดล้อมและสุขภาพของมนุษย์ อีกทั้งยังลดต้นทุนในการกระบวนการผลิตอาหารแบบปลอดเชื้อด้วย

Keywords: Condensation, Concentration, Heat transfer, Heat exchanger, Hydrogen peroxide
คำสำคัญ: การควบแน่น ความเข้มข้น การถ่ายเทความร้อน ชุดแลกเปลี่ยนความร้อน ไฮโดรเจนเปอร์ออกไซด์

[1]*Correspondent author:b_sittipong02@hotmail.com*
* *Student, Doctor of Philosophy Program in Chemical and Environmental Engineering, Burapha University*
** *Asst. Prof. Department of Chemical Engineering, Faculty of Engineering, Burapha University*
*** *Assoc. Prof. Department of Mechanical Engineering, Faculty of Engineering, Burapha University*

Introduction

Today, the demand for hydrogen peroxide (H_2O_2) is increasing dramatically owing to the rapid expansion of the aseptic food industry and other allied businesses. The demand for H_2O_2 is forecasted to reach 4.67 million metric tons by 2017 [1]. In the aseptic food industry, concentrated (35% w/w) H_2O_2 liquid is used in fill pack ultra-high temperature (UHT) processes in order to increase the shelf life of packaged food [2]. The vapor, which contains high concentrations of H_2O_2, is generated and fed continuously into the filling aseptic process technology. Specifically, H_2O_2 vapor is used to stop the growth of micro-organisms and sterilize food during the filling and packing process in the aseptic zone. Subsequently, the exhaust gases with excessive amounts of H_2O_2 present in the vapor mixture leaves the aseptic zone and is discharged directly from the production area to the environment outside of the packaging plant. While portions of the emitted H_2O_2 laden vapors, which have highly oxidizing properties, will undergo decomposition reactions in the atmosphere, other portions can be deposited on building roofs and walls, and nearby vegetation such as trees; this can be detrimental to these structures. Moreover, the vapors may also impact the health of neighboring communities as exposures to H_2O_2 may lead to inflammation in the eyes, nose, throat, and lungs; such exposures can also cause skin irritation [3].

In order to reduce the impact of H_2O_2 emissions into the environment and on human health, the production process should be altered to reduce the H_2O_2 concentration in the released exhaust gases. Such a process would ideally involve the recovery of the H_2O_2 and H_2O in the vapor mixture from the exhaust gases, where it could recycle and reuse in the production process. This would not only help to protect environmental quality, but it would also significantly reduce the consumption of H_2O_2, during food processing, as well as the maintenance costs for the scrubber system. On the basis of this idea, heat exchanger techniques can potentially be used in the recovery process of exhaust gases comprised of two condensable species: hydrogen peroxide vapor (H_2O_2), water vapor (H_2O)

A literature review was performed and found that many researchers had studied heat transfer condensation processes. They introduced a mathematical model in ANSYS CFD for non-condensable substances and someone introduced one specie condensation [4-9]. Some other researcher studied heat transfer and condensation of one condensable specie in tube bundle and heat exchanger [10-14]. The researchers have not yet studied the condensation of H_2O_2 mixture.

However, a two condensable species system would be complicated given that the two condensable components would display different physical properties upon phase change. Furthermore, an exhaust gas system containing three species, such as H_2O_2, H_2O, and air, (i.e., two condensing species, namely, H_2O_2 vapor and water vapor, and non-condensable air), would be a significantly complicated system to work with as compared to the single species condensation process investigated by previous researchers.

Objective of this study

To investigate the effect of inlet temperature and flow rate of cold water on condensation of exhaust gases with two condensing species (H_2O and H_2O_2) in a four in-line tube bundle heat exchanger.

Methodology

In this study, the condensation and concentration rates of mixing two condensable species were investigated with the test section by taking two study cases to compare the results with the computation model (species transport model, STM) study in ANSYS Fluent software. After that, we made the additional experiment with the test section in order to get the condensation figures of the other cold water conditions. In each experiment, it was fixed for the exhaust gas conditions (The mass percentage of the exhaust gas composition at the inlet H_2O_2:H_2O:air was 4.5%, 32.6%, and 62.9%, flow rate of 90 m^3/h, temperature of 45°C and pressure of 1 atm.) and varied the cold water conditions (three different flow rates: 4 L/min, 7.5 L/min, 11 L/min and four different temperatures: 10°C, 15°C, 20°C, 25°C and fixed pressure at 1.48 atm.).

Test section

The heat exchanger consists of four in-line tube bundles as shown in **Figure 1** was designed as a 1.5 m long horizontal square duct chamber with dimensions of 115 × 115 mm.[2] and it has an entry grill and baffle plates; the exchanger was fabricated by using stainless steel material. The dimensions of the tubes are as follows: outside diameter of the tube,18 mm; tube thickness, 1 mm; tubes lengths, 115 mm; transverse and longitudinal pitch of the tubes, 25 mm. A total of 32 tubes were packed in one bundle and the tube material was stainless steel. The baffle plate between each tube bundle plays a crucial role in regulating hot exhaust gas flow and improves heat transfer between the hot exhaust gases and the cold water in the tube bundles. Cold water is supplied through the inlet stainless steel pipe which has an outside diameter of 33.7 mm and a thickness of 2.6 mm.

This heat exchanger is equipped with a test section where the condensation takes place is shown in **Figure 2.** The hot fluid, i.e., the H_2O_2–air vapor mixture, is supplied by the exhaust generator (No. 1) to the test section through the inlet pipe. A suction blower (No. 5) is connected to the outlet chamber and sucks the vapor through the outlet exhaust pipe (No. 6). The hot vapor then flows through the heat exchanger (No.2) which consists of four bundle cooling in-line tube arrangement (No.3). The holes at the inlet and outlet positions of the chamber provide access to tools that can measure the temperature, pressure, velocity, and concentration of the fluids (No. 9). The cooling unit supplies cold water from a 57 L capacity water tank (No. 8). The pressure and flow rate of the inlet cold water are controlled by a pump and a control valve (No. 11), respectively. Cold water is supplied through the inlet stainless steel pipe (No. 10) through four bundled tubes arranged in series and returns back to the water tank. Sensors (No. 12) are installed at the inlet and outlet pipes, and these measure the temperature, pressure, and flow rate. The condensate liquid occurs at the cooling tube surface because of the heat exchange during the cross flow, wherein the cold fluid takes out the heat from the hot fluid until the temperature is

lower than the saturation temperature. It drops down from each tube bundle into the collection bottom tray (No. 4), and then, it flows down to the collection tank (No. 7).

The exhaust gas was fed into the inlet at a velocity of 3.6 m/s. (calculated from the volumetric flow rate of 90 m^3/h based on the cross sectional area of the inlet pipe), a temperature of 45°C and an atmospheric pressure of 1 atm. This exhaust gas consists of three components as follow: condensable hydrogen peroxide (4.5% mass), condensable water vapor (32.6% mass), and non-condensable air (62.9% mass). The corresponding mass flow rate of each species was H_2O_2 vapor 4.17 kg/h, H_2O vapor 20.12 kg/h, and air 56.50 kg/h, respectively. The inlet pressure of cold water was 1.48 atm. Condensation and convection heat transfer were studied at the following four different temperatures: 10°C, 15°C, 20°C, and 25°C; three discrete flow rates amounting to 4 L/min, 7.5 L/min, and 11 L/min were also tested. Note that the test section has a cross-flow scheme wherein the cold water flows perpendicular to the flow direction of the exhaust gas.

Computational model

Initially, the 3D geometry was created for the same dimension as heat exchanger used in the test section. The design of this heat exchanger is shown the geometry and dimension in Figure 1. It consists of four tube bundles (each in-line tube arrangement as shown in Figure 3). The fluid flow is the cross-flow arrangement, the exhaust gases and water flow at right angles to each other.

In this study, the relatively simplicity of the species transport model (STM) is shown in the Figure 4, for the simulation of the heat and mass transfer in the heat exchanger. H_2O vapor and H_2O_2 vapor in the exhaust gases zone are condensed when it is in contact with the cold surface of the solid zone (tube wall). The condensation occurs in the form of a smooth film, which flows down the surface under the action of the gravity. The presence of a liquid film over the solid zone constitutes a thermal resistance to the heat flow. Exhaust gases are represented by a mixture of three major species, H_2O_2, H_2O, and air, with the air specie considered as a non-condensable gas. Analytical modeling in this study was developed with the assumptions and simplifications as follows: Steady state one dimensional flow, two phase flow (gas and liquid) for the exhaust gas side and one phase flow for the cooling water side, film condensation only occurs on the tube wall surface, the thermal resistances due to the film and tube wall are negligible, the heat exchanger is well-insulated so that heat loss to surroundings is negligible and thus heat transfer from the hot fluid is equal to the heat taken out by cold water, no chemical reactions, change in the kinetic and potential energies of fluid exhaust are negligible and fluid properties are constant. The commercial code ANSYS FLUENT software was used to support simulation of the experiment. Boundary conditions specify the flow and thermal variables on the boundaries of the physical domain (Figure 5) shows the boundary condition utilized in this study.

The governing equations for the continuity equation for the mixture [15] can be expressed as follows:

$$\frac{\partial}{\partial t}(\rho_m) + \nabla \cdot (\rho_m \vec{v}_m) = 0 \quad (1)$$

where $\rho_m$is the mixture density and $\vec{v}_m$ is the mass-averaged velocity which can be defined as:

$$\vec{v}_m = \frac{\sum_{k=1}^{n} \alpha_k \rho_k \vec{v}_k}{\rho_m} \quad (2)$$

$$\rho_m = \sum_{k=1}^{n} \alpha_k \rho_k \quad (3)$$

where α_k is the volume fraction of phase *k.*

The momentum equation for the mixture can be obtained by summing the individual momentum equations for all phases. It can be express as:

$$\frac{\partial}{\partial t}(\rho_m \vec{v}_m) + +\nabla \cdot (\rho_m \vec{v}_m) = -\nabla p + \nabla\left[\mu_m\left(\nabla \vec{v}_m + \nabla \vec{v}_m{}^T\right)\right] + \rho_m \vec{g} + \vec{F} + \nabla \cdot \left[\sum_{k=1}^{n} \alpha_k \rho_k \vec{v}_{dr,k} \vec{v}_{dr,k}\right] \quad (4)$$

Where *n* is number phases, $\vec{F}$ is a body force, μ_m is the viscosity of the mixture, and $\vec{v}_{dr,k}$is the drift velocity for secondary phase *k.* These viscosity and drift velocity can be defined as:

$$\mu_m = \sum_{k=1}^{n} \alpha_k \mu_k \quad (5)$$

$$\vec{v}_{dr,k} = \vec{v}_k - \vec{v}_m \quad (6)$$

Conservation of species is predicted by the local mass fraction of each species, Y_i, through the solution of a convection-diffusion equation for the i^{th} species. This conservation equation takes the following form:

$$\frac{\partial}{\partial t}(\rho Y_i) + \nabla \cdot (\rho \vec{v} Y_i) = -\nabla \cdot \vec{J}_i + R_i + S_i \quad (7)$$

where R_i is the net rate of production of species *i* by chemical reaction, S_i is the rate of creation by addition from the dispersed phase plus any user-defined sources and $\vec{J}_i$ is the diffusion flux of species *i*. The diffusion flux can be written as:

$$\vec{J}_i = -\rho D_{m,i} \nabla Y_i - D_{T,i} \frac{\nabla T}{T} \quad (8)$$

Here $D_{m,i}$ is the mass diffusion coefficient for species *i* in the mixture, and $D_{T,i}$ is the thermal diffusion coefficient for species *i*.

The energy equation for the mixture takes the following form:

$$\frac{\partial}{\partial t}(\rho E) + \nabla \cdot (\vec{v}(\rho E + p) = \nabla \cdot \left(\lambda_{eff} \nabla T - \sum_i h_i \vec{J}_i + (\bar{\bar{\tau}}_{eff} \cdot \vec{v})\right) + S_h \quad (9)$$

where λ_{eff} is the effective conductivity ($\lambda + \lambda_t$, where λ_t is the turbulent thermal conductivity, defined according to the turbulence model being used). The terms $\left(\lambda_{eff} \nabla T - \sum_i h_i \vec{J}_i + (\bar{\bar{\tau}}_{eff} \cdot \vec{v})\right)$ represent energy transfer due to conduction, species diffusion, and viscous dissipation, respectively. S_h includes the heat of chemical reaction, and any other volumetric heat sources. The total energy per unit mass can be defined as:

$$E = h - \frac{p}{\rho} + \frac{v^2}{2} \quad (10)$$

where sensible enthalpy *h* is defined for compressible flows as

$$h = \sum_i Y_i h_i \quad (11)$$

and for incompressible flow as

$$h = \sum_i Y_i h_i + \frac{p}{\rho} \tag{12}$$

the enthalpy of the component *i* described by the equation:

$$h_i = \int_{T_{ref}}^{T} c_{p,i} dT \tag{13}$$

where T_{ref} is 298.73 K and $c_{p,i}$ is the heat capacity of at constant pressure for species *i* in the mixture.

Results

Model validation study has been carried out by using the experimental data comparing with computational results in two cases (Case A and Case B). Table 1 shows the comparison of the average values of water exit temperature, exhaust gas exit temperature, and exhaust gas exit mass fraction of H_2O and H_2O_2 obtained by the experiment from the test section and the computational model (species transport model, STM). In both cases the experiments showed the heat exchange figures that the exhaust gas exit temperature of case A reduced from 45 °C to 31.4 °C (decreased 13.6 °C) and case B reduced from 45 °C to 37.7 °C (decreased 7.3 °C). In the cold water side, the exit temperature of case A increased from 10 °C to 20.8 °C (increased 10.8 °C) and case B increased from 25 °C to 32.6 °C (increased 7.6 °C). Condensation liquid of component H_2O and H_2O_2 were consistently measured comparing with the exit mass fraction of these both components in the exhaust gas. Condensed liquid is mixed between condensed H_2O and condensed H_2O_2 that case A is higher than case B. H_2O_2 concentration in condensed liquid of case A is lower than case B. It is the same trend of STM results. The results of the comparison in the table shown the errors are within the ranges of -6.3 to 8.5%.

After passing the validation of the test section and computation model, we made the additional test with the other conditions of four different inlet temperatures: 10°C, 15°C, 20°C, 25°C and three different flow rates of cold water: 4 L/min, 7.5 L/min, 11 L/min. From this addition test, we got the different condensation results of mixing species H_2O and H_2O_2. Figure 6 illustrates the condensation rate. The trend in the condensation rate was consistent with the theory of heat and mass transfer, and it was aligned with the trends for the mass flux and mass fraction of H_2O and H_2O_2. The total condensation rate increased when the inlet cold water temperature was decreased or the flow rate was increased. It makes the heat transfer rate increasing from the exhaust gas go to cold water. This is because the interfacial temperature will be decreased which makes increasing of temperature difference and concentration difference between the exhaust gas and the liquid film condensation. Therefore, convective heat transfer rate of exhaust gases $[h_{eg}A(T_{eg} - T_{inf})]$ and convective mass transfer rate $[k_m h_{fg} A(y_i - y_{inf})]$ also increase.

The condensation rate of both species H_2O_2 and H_2O at varying temperatures and flow rate of cold water (Figure 7) were reduced when the cold water inlet temperature was increased and the flow rate was decreased. Thus, higher condensation rates can be achieved by lowering the temperature or increasing the flow rate of the cooling water. The maximum condensation rate of 6.39 kg/h was achieved with a cold water flow rate

of 11 L/min at 10°C consists of H_2O_2 1.31 kg/h and H_2O 5.08 kg/h while the minimum condensation rate of 2.78 kg/h was observed with cold water flow rate of 4 L/min at 25°C consisting of H_2O_2 0.65 kg/h and H_2O 2.13 kg/h. Therefore, we can calculate the percentage of H_2O_2 condensation comparing with the inlet H_2O_2 in the exhaust gas that the maximum condensation is 31.4% and minimum is 15.6%

Mixing of condensed liquid H_2O_2 and H_2O in each experiment condition was measured the H_2O_2 concentrations (Figure 8). Again, the H_2O_2 concentrations showed an increasing trend when the temperature and flow rate of the cooling water increased. It is consistent with the increasing of condensation ratio between condensed H_2O_2 and condensed H_2O. The maximum H_2O_2 concentration in the condensed liquid was observed with a cold water flow rate of 11 L/min at 25°C; the concentration was 33%. The minimum H_2O_2 concentration was observed with a cold water flow rate of 4 L/min at 10°C; the concentration was 16%.

Discussion and conclusions

On the basis of the data obtained from the test-rig and simulation model discussed in this work, the following conclusions can be drawn.

1. The multi-species transport model has been developed for the simulation of condensing unit which shows the results of a validation model comparing with experimental errors are within the ranges of -6.3 to 8.5% which the STM agrees with the experimental data fairly well. This agreement is based on a review of published literature resulted in the accuracy of simulation prediction compared to experimental results [16]. It is defined the percentage bias (PBIAS) that they suggested two less stringent ratings of below 10% is “good” and below 20% is “acceptable”.

2. This study demonstrates that concentrations of H_2O_2 in the released exhaust gas can be reduced by condensation process in a heat exchanger. Thus, this technology could help to reduce the impact of H_2O_2 emissions from food processing operations on the environment and human health. The dependency of the condensation rate and concentration of condensate from the exhaust gas on the flow rates and temperatures of the cold water were observed to be as follows:

2.1 The condensation rate of H_2O_2 depends on the heat transfer rate which effected by flow rate and inlet temperature of the cold water. The maximum H_2O_2 condensation rate is 31.4% at cold water flow rate of 11 L/min at 10° while the minimum H_2O_2 condensation rate is 15.6% was observed with a cold water flow rate of 4 L/min at 25°C. Therefore, this result suggests that a higher condensation rate is depended on cold water with high flow rate and low a temperature.

2.2 The H_2O_2 concentration rate is consistent with the condensation ratio between H_2O_2 and H_2O. The maximum H_2O_2 concentration rate in the condensed liquid was observed with cold water flow rate of 11 L/min at 25°C; the concentration was 33%. The minimum H_2O_2 concentration rate was observed with cold water flow rate of 4 L/min at 10°C; the concentration was 16%. More condensed H_2O at lower flow rate and inlet temperature will

be diluted H_2O_2 concentration down. Therefore, this result suggests that higher concentration rate is depended on cold water with high flow rate and high temperature.

References

1. San J. Global hydrogen peroxide market to reach 4.67 million metric tons by 2017 [Internet]. 2016 [updated 2016 June 07; cited 2016 Aug 15]. Available from: http://www.prweb.com/releases /hydrogen_peroxide/bleaching_pulp_paper/prweb9268178.htm
2. Von Bockelmann BAH, Von Bockelmann ILI. Aseptic packaging of liquid food products: a literature review. Journal of Agricultural and Food Chemistry. 1986; 34(3): 384–392.
3. Vomela J. Steam condensation in presence of noncondensable gas. Heat Transfer Research. 1997; 28(4–6): 289–295.
4. Zschaeck G, Frank T, Burns A. CFD modelling and validation of wall condensation in the presence of non-condensable gases. Nucl Eng Des. 2014; 279: 137–146.
5. Yaïci W, Ghorab M, Entchev E. 3D CFD analysis of the effect of inlet air flow maldistribution on the fluid flow and heat transfer performances of plate-fin-and-tube laminar heat exchangers. Int J Heat Mass Transf. 2014; 74: 490–500.
6. Mimouni S, Foissac A, Lavieville J. CFD modelling of wall steam condensation by a two-phase flow approach. Nucl Eng Des. 2011; 241(11): 4445–4455.
7. Vyskocil L, Schmid J, Macek J. CFD simulation of air–steam flow with condensation. Nucl Eng Des. 2014; 279: 147–157.
8. Li JD. CFD simulation of water vapour condensation in the presence of non-condensable gas in vertical cylindrical condensers. Int J Heat Mass Transf. 2013; 57(2): 708–721.
9. Iacovides H, Launder B, West A. A comparison and assessment of approaches for modelling flow over in-line tube banks. Int J Heat Fluid Flow. 2014; 49: 69–79.
10. Li X, Wu X, He S. Numerical investigation of the turbulent cross flow and heat transfer in a wall bounded tube bundle. Int J Therm Sci. 2014; 75: 127–139.
11. Groff MK, Ormiston SJ, Soliman HM. Numerical solution of film condensation from turbulent flow of vapor–gas mixtures in vertical tubes. Int J Heat Mass Transfer. 2007; 50: 3899–3912.
12. Yuann RY. Condensation from vapor–gas mixture for forced downflow Inside a Tube. 1st ed. Berkeley: University of California; 1993.
13. Panday JA. Two-dimensional turbulent film condensation of vapours flowing inside a vertical tube and between parallel plates: a numerical approach. Int J Refrig. 2003; 26: 492–503.
14. Lin CX, Wang D, Bao A. Numerical modeling and simulation of condensation heat transfer of a flue gas in a bundle of transport membrane tubes. International Journal of Heat and Mass Transfer. 2013; 60: 41–50.
15. ANSYS Inc. ANSYS CFX-Solver Theory Guide. Canonsburg: Southpointe; 2013.

16. Moriasi DN, Arnold JG, Van Liew MW, Bingner RL, Harmel RD, Veith TL. Model evaluation guidelines for systematic quantification of accuracy in watershed simulations. Transactions of the ASABE. 2007; 50: 885-900.

NOMENCLATURE

A	surface area (m^2)
c_p	heat capacity at constant pressure (J/kg-K)
D	mass diffusion coefficient (m^2/s)
E	total energy (J)
$\vec{F}$	force vector (N)
$\vec{g}$	gravitational acceleration (m/s^2)
h	enthalpy (J/kg)
h_{fg}	latent heat (J/kg)
$\vec{J}$	diffusion flux (kg/m^2)
k_m	mass transfer coefficient (kg/s m^2 mol)
p	pressure (Pa)
S_T	tube transversal pitch (m)
S_L	tube longitudinal pitch (m)
t	time (s)
T	temperature $(°\mathrm{C})$
Y	mass fraction (dimensionless)
y	mole fraction (dimensionless)
Greek symbols	
$\vec{v}$	overall velocity vector (m/s)
α	volume fraction (dimensionless)
λ	thermal conductivity (W/m K)
μ	dynamic viscosity (kg/m-s)
ρ	density (kg/m^3)
$\bar{\bar{\tau}}$	stress tensor (Pa)
Subscripts	
dr	drift velocity
eg	exhaust gas
i	species *i*
inf	interfacial
k	phase *k*
m	mixture

Table 1 Comparison between experimental and computational results

	Case A			Case B		
	Exp.	STM	Error (%)	Exp.	STM	Error (%)
Exhaust gas exit temperature (°C)	31.40	33.00	5.1	37.70	38.80	2.9
Cold water exit temperature (°C)	20.80	21.80	4.8	32.60	31.00	-4.9
H_2O vapor exit mass fraction (%)	2.12	2.24	5.7	2.64	2.49	-5.6
H_2O_2 vapor exit mass fraction (%)	0.26	0.25	-3.4	0.24	0.26	8.5
H_2O condensation rate (kg/h)	3.82	4.10	7.3	2.32	2.20	-5.2
H_2O_2 condensation rate (kg/h)	0.84	0.80	-4.8	0.64	0.60	-6.3
H_2O_2 concentration in condense liquid (%)	17.10	16.10	-5.8	24.40	25.20	3.3

Case A conditions: $P_{eg,in}$= 1 ATM , $T_{eg,in}$= 45°C, $Y_{H_2O,in}$= 2.8%, $Y_{H_2O_2,in}$= 0.31%, $u_{eg,in}$= 3.6 m/s, $T_{wt,in}$= 10°C, $u_{wt,in}$= 4 l/min.

Case B conditions: $P_{eg,in}$= 1 ATM, $T_{eg,in}$= 45°C, $Y_{H_2O,in}$= 2.8%, $Y_{H_2O_2,in}$= 0.31%, $u_{eg,in}$= 3.6 m/s, $T_{wt,in}$= 25°C, $u_{wt,in}$= 11 l/min.

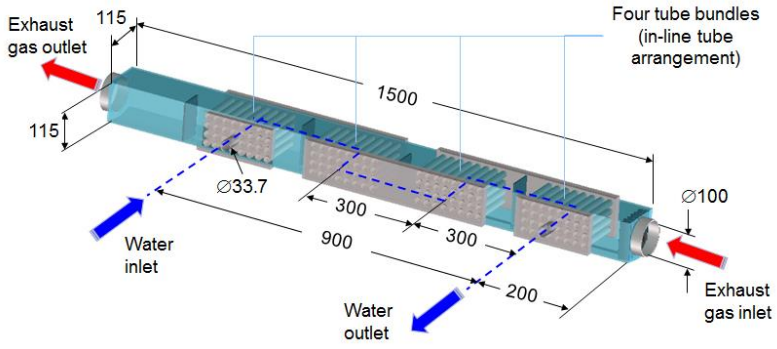

Figure 1 Heat exchanger with four in-line tube bundles

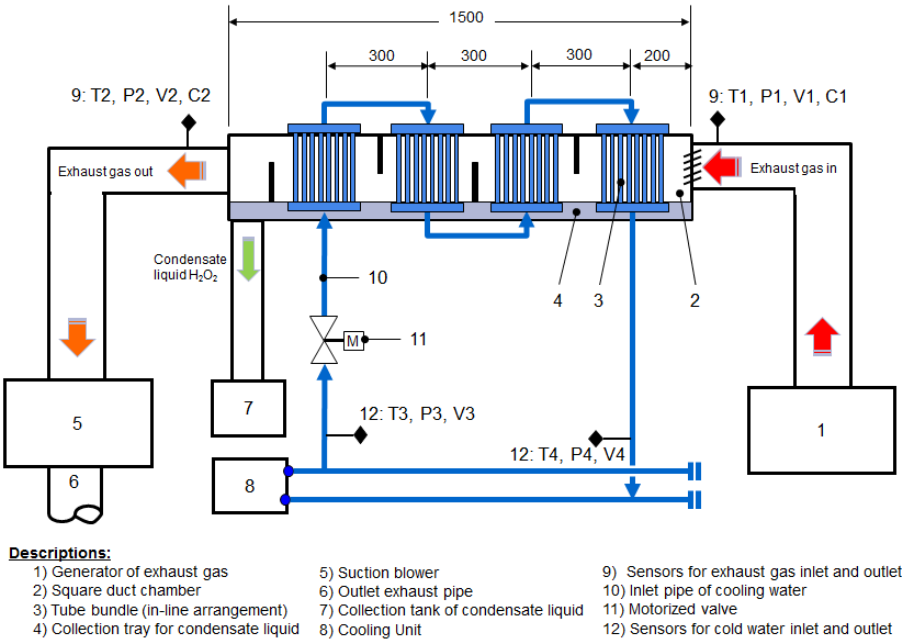

Figure 2 Test section where H_2O_2 and H_2O condensation occurs

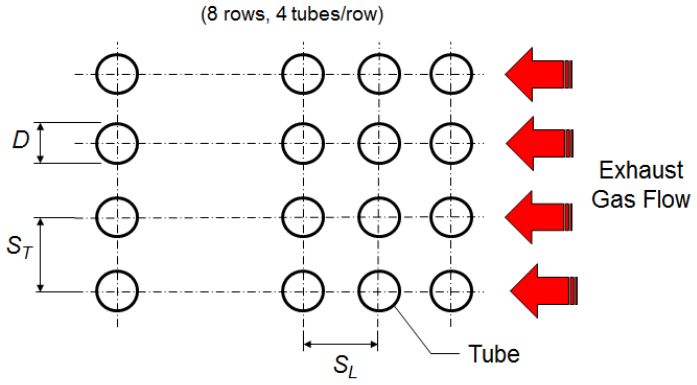

Figure 3 In-line tube bundle

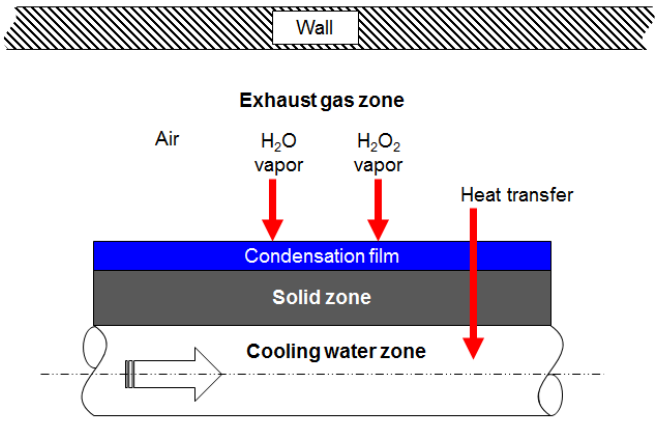

Figure 4 The species transport model

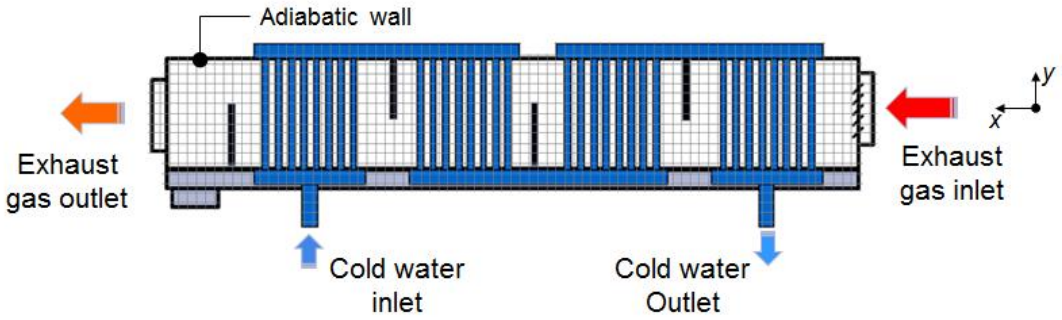

Figure 5 Boundary condition

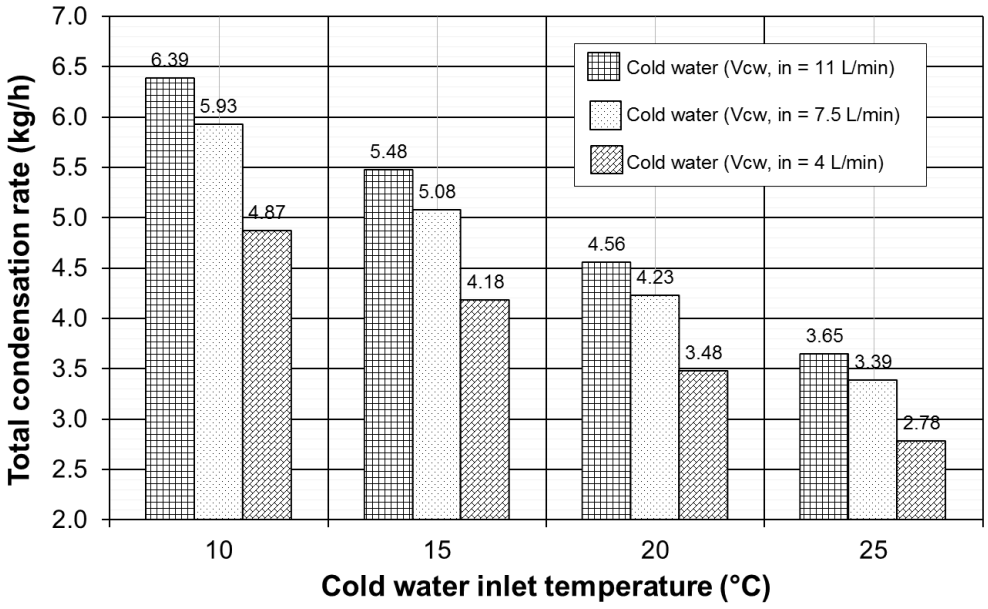

Figure 6 Total condensation rates of mixing species H_2O_2 and H_2O.

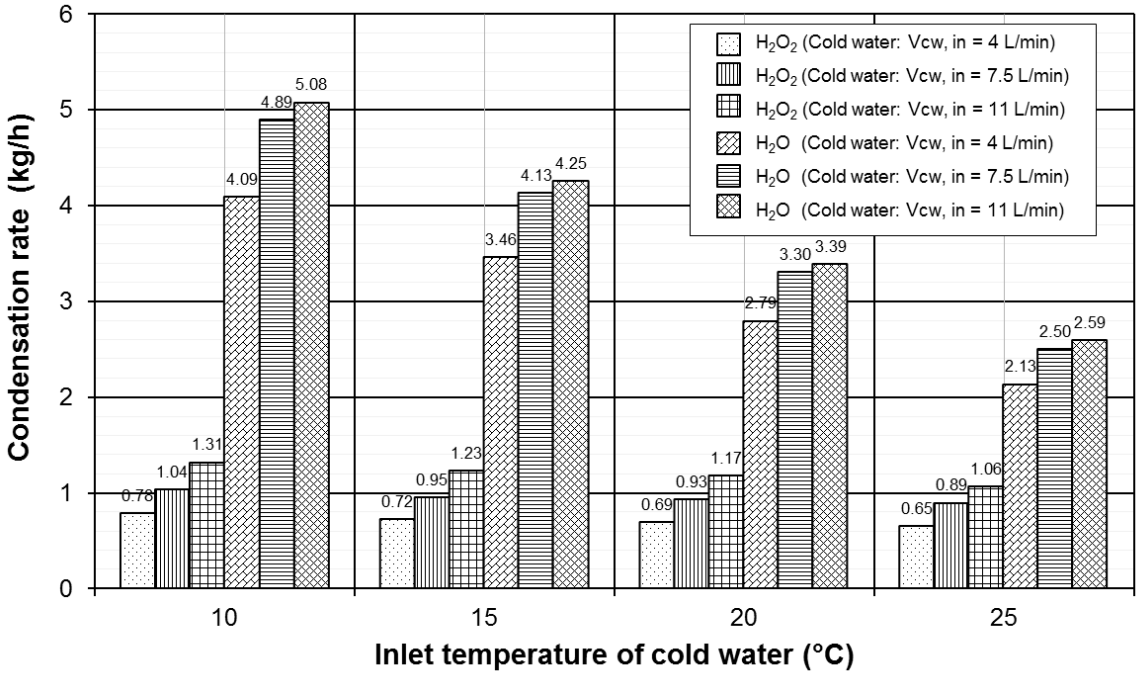

Figure 7 Condensation rates for H_2O_2 and H_2O.

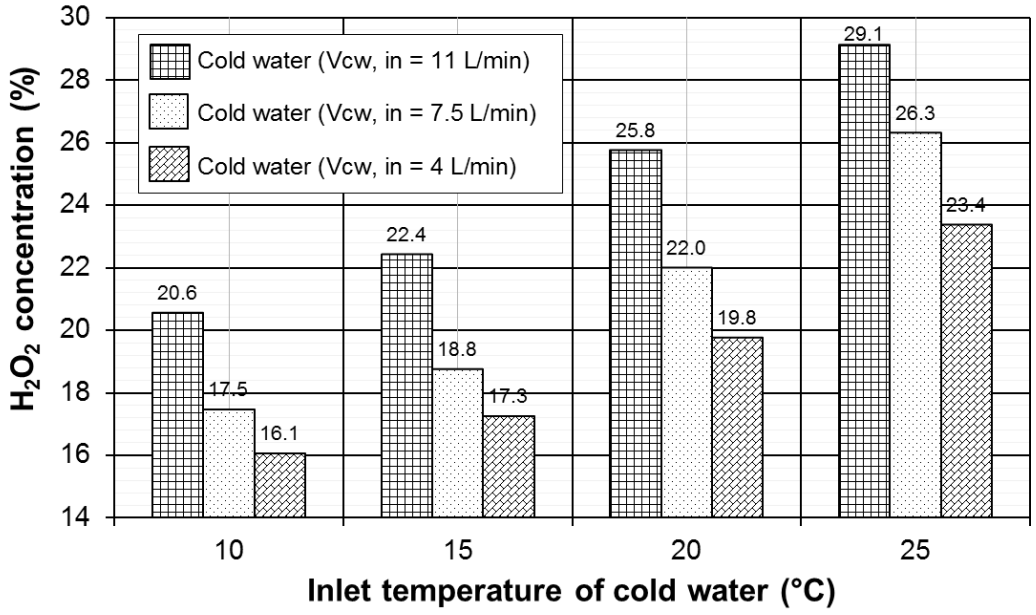

Figure 8 H_2O_2 concentrations in condensed liquid for varying inlet cold water temperatures.